Measurement of excited-state lifetime using two-pulse photon echoes in rubidium vapor

E. A. Rotberg, B. Barrett, S. Beattie, S. Chudasama, M. Weel, I. Chan, and A. Kumarakrishnan

Department of Physics and Astronomy, York University, Toronto Ontario M3J 1P3, Canada

Received July 26, 2006; revised October 4, 2006; accepted October 4, 2006;
posted October 20, 2006 (Doc. ID 73314); published February 15, 2007

We report a measurement of the $5P_{3/2}$ excited-state lifetime using two-pulse photon echoes in Rb vapor. The measurement is precise to ~1% and agrees with the best measurement of atomic lifetime in Rb. The results suggest that a measurement precise to ~0.25% is possible through additional data acquisition and study of systematic effects. The experiment relies on short optical pulses generated from a cw laser using acousto-optic modulators. The excitation pulses are on resonance with the $F=3\rightarrow F'=4$ transition in ^{85}Rb or the $F=2\rightarrow F'=3$ transition in ^{87}Rb. The resulting photon echo signal is detected using a heterodyne detection technique. The excited-state lifetime is determined by measuring the exponential decay of the echo intensity as a function of the time between the excitation pulses. We also present a study of the echo intensity as a function of excitation pulse area and compare the results to simulations based on optical Bloch equations. The simulations include the effects of spontaneous emission as well as spatial and temporal variations of the intensities of excitation pulses.

OCIS codes: 020.1670, 020.490, 300.6240.

1. OVERVIEW

Knowledge of atomic lifetimes is essential for a wide range of experiments in laser spectroscopy, such as atom and ion trapping,[1] trace-gas analysis, and remote sensing. Precision measurements are also essential for testing quantum-mechanical calculations of level structures.[2–4]

Precision measurements of natural linewidths and atomic lifetimes have generally involved scanning a probe laser with a narrow linewidth or observing the decay of the atomic fluorescence using photon-counting techniques. The dominant systematic effects in these experiments are the contributions of laser linewidth and radiation trapping. As a result, these experiments have required the development of sophisticated experimental setups. In this paper we show the suitability of a widely established coherent transient technique, namely the photon echo, for obtaining a precision measurement of an atomic lifetime. This is a well-known technique for canceling the effect of atomic velocity distribution and has the advantage of being insensitive to the effects of radiation trapping and laser linewidth.

During the past ten years, several techniques have been perfected for precision measurements of atomic lifetimes. In Ref. 5 a laser with a linewidth of only a few kilohertz was used to measure the natural linewidth in a sample of velocity selected laser-cooled Na atoms to a precision of ~0.25%. This technique requires the development of a laser with a narrow linewidth. Such lasers have been constructed in only a small number of groups. An alternative technique for measuring the atomic lifetime with comparable precision involves exciting a sample of trapped atoms with a laser pulse and observing the fluorescence decay using photon-counting techniques.[6] This requires specialized expertise to detect small numbers of photons and develop suitable counting electronics. In contrast, the photon echo technique does not involve these challenges and can be widely accessible to a large number of experimental groups. Other techniques that have been developed include photoassociation spectroscopy[7] and fast atomic beam experiments.[8,9]

Although photon echoes have been used extensively to measure relaxation rates in atomic and molecular species,[10] collisional rates,[11] diffractive collisions,[12] atomic level structure,[13] and lifetimes in solids and doped crystals,[14,15] to the best of our knowledge, it has not been used for atomic lifetime measurements.

In this paper, we demonstrate a precision measurement of the relatively short-lived lifetime (~27 ns) of the $5P_{3/2}$ levels in Rb vapor. We have also investigated a number of potential systematic effects. We report a measurement that is precise to ~1% and show that a precision of ~0.25% is realistically attainable by accumulating more data following a detailed understanding of systematic effects. We have also investigated the echo intensity as a function of the excitation pulse areas. We compare our results to numerical simulations of the optical Bloch equations for a two-level system.

The rest of this paper is organized in the following manner: In Section 2, we discuss the concepts related to the photon echo and present the functional dependence of the signal intensity on the time separation between the excitation pulses. Section 3 contains experimental details and a description of the procedure for extracting the lifetime. Section 4 is devoted to results and discussion associated with the precision measurement of the lifetime. In the same section, we also present the measured dependence of the echo signal intensity as a function of excitation pulse areas. The results are compared to numerical simulation based on the theory of two-level atoms. The details of the simulations are presented in Appendix A.

0740-3224/07/030671-10/$15.00

2. THEORETICAL CONCEPTS

Spin echoes[16] and photon echoes[17] are well understood and have been studied extensively over the past 50 years. In a typical photon echo experiment involving dilute atomic gases, a laser pulse is applied at $t=0$ to create a coherent superposition of ground and excited states.[18] Owing to Doppler broadening, the superposition dephases with time. At $t=T$ a second pulse is applied and rephases the superposition so that dipole radiation occurs at $t=2T$ (photon echo). The decay of the echo signal as a function of T can be used to measure various relaxation effects.

The basic properties of a two-level atom and its interaction with an external electric field are based on the treatment in Refs. 18–20. This treatment can be used to describe coherent transient effects such as free induction decay and photon echoes using a semiclassical Bloch vector model.

In a typical photon echo experiment involving an inhomogeneously broadened sample, a $\pi/2$ pulse applied at $t=0$ will rotate the Bloch vector associated with the macroscopic dipole moment to the uv plane. Following the pulse, the Bloch vectors associated with the individual atoms will precess freely around the w axis. Owing to Doppler broadening, the precession occurs with different rates for different atoms, resulting in rapid dephasing of the macroscopic dipole moment free induction decay. It is possible to reverse the dephasing process after some time $t=T$ using a π pulse. This creates a rephased dipole moment resulting in an echo at time $t=2T$. A schematic representation of the process of echo formation is shown in Fig. 1.

For a Doppler broadened gas, in the absence of collisional dephasing, the echo intensity depends only on radiative decay. This dependence is given by

$$I = I_0 \exp\left[-\frac{2T}{\tau}\right]. \tag{1}$$

The laser linewidth and the temporal shape of the excitation pulses determine the velocity distribution that contributes to the echo formation. Although these factors affect the signal strength, they do not affect the decay time constant. Similarly, the intensity, temporal shape of the excitation pulses, and sample density affect the echo amplitude and pulse propagation but not the decay time constant. Spontaneous emission during the excitation pulses is also not expected to affect the decay time constant.

3. EXPERIMENTAL SETUP

In photon echo experiments, it is necessary to use excitation pulses that are shorter than the excited-state lifetime. This will limit the effects of spontaneous emission on the evolution of the echo. Previous experiments[11] were performed using short dye laser pulses that excited the entire Doppler profile. To make a lifetime measurement, it is necessary to measure the echo amplitude as a function of time delay between the excitation pulses. In experiments with dye lasers it is difficult to control the delay time owing to the jitter associated with the laser Q switches and the inconvenience of adding optical delays. Therefore, photon echo measurements have generally been confined to measuring collisional rates[11] and lifetimes of long-lived relaxation rates.[10]

We have used a cw Ti:sapphire ring laser as a source of the excitation pulses. The laser has a linewidth of $\sim$1.5 MHz. The linewidth was inferred by measuring the beat note between this laser and a grating stabilized diode laser.

The laser beam is sent through a chain of acousto-optic modulators (AOM) to derive the different laser frequencies used in the experiment. The optical pulses are generated by pulsing the AOMs.

Frequency locking is achieved by diverting a small portion of the laser light through a dual-pass AOM into a saturated absorption spectrometer. The dual-pass AOM

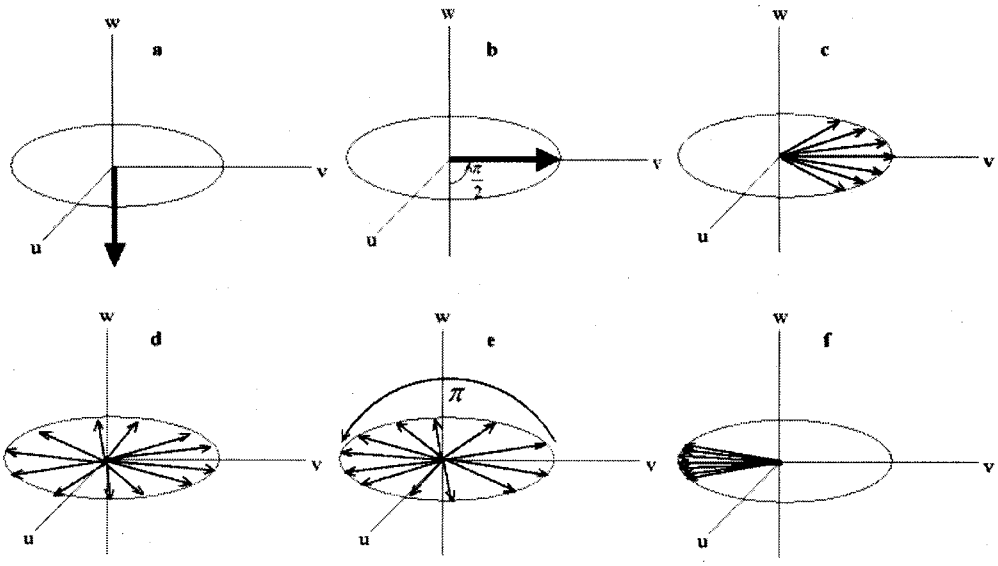

Fig. 1. Bloch vector representation. (a) Macroscopic Bloch vector representing all atoms in the ground state. (b) Superposition state immediately after $\pi/2$ pulse. (c), (d) Bloch vector dephasing. (e) Inversion due to π pulse. (f) Bloch vector rephasing (photon echo).

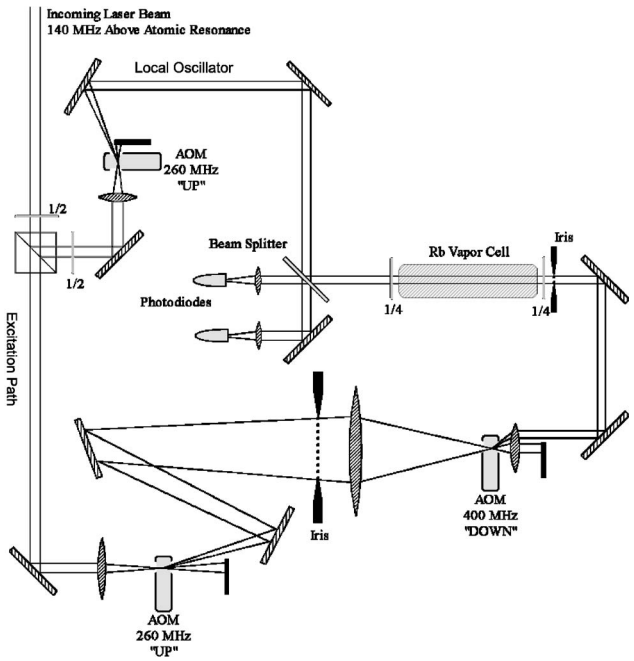

Fig. 2. Optical layout. 1/2 and 1/4 represent $\lambda/2$ and $\lambda/4$ wave plates, respectively.

operates at 70 MHz. The laser is modulated and is locked to within 1 MHz to the appropriate Doppler-free hyperfine peak using a lock-in amplifier. This ensures that the laser beam directed to the experiment is 140 MHz above the $F=3\rightarrow F'=4$ transition in ^{85}Rb or the $F=2\rightarrow F'=3$ transition in ^{87}Rb. Since the excited state is a $5P_{3/2}$ level in both isotopes, it can be estimated that any isotopic dependence is negligible, since the ratio of the isotropic energy difference to the optical frequency is $\sim 10^{-5}$. To check for possible systematic errors in our technique, we carry out the experiment in both isotopes.

The photon echo is generated in a 7 cm long vapor cell containing a natural abundance of Rb isotopes ($\sim$72% of ^{85}Rb and $\sim$28% of ^{87}Rb). The vapor density can be varied by heating the cell to the desired temperature. Because the optical windows of the cell are made from thicker glass than the rest of the vapor cell, the windows are heated individually by tape heaters placed around them. Thus, we avoid the possibility of coating the cell windows with Rb.

The cell was wrapped in thermally insulating material and placed inside a solenoid. The solenoid containing the cell was placed inside a box, which further thermally insulated it from the environment. Circularly polarized excitation pulses were used, and the solenoid was used to provide a weak quantizing magnetic field of $\sim$1 G.

It was possible to achieve temperatures of $\sim 30^\circ$C using the heating tape alone. To heat the cell to a higher temperature, we used a variable hot-air blower and directed the air stream into the box containing the cell. Thus, we were able to achieve temperatures as high as 60°C. The temperature was monitored using a digital thermometer with the sensor attached to the side of the cell. Under typical operating conditions, the cell temperature was stable to within $\pm 2^\circ$C.

To verify the change in vapor density as a function of temperature, we scanned a weak probe laser across the atomic resonance and observed the change in the Doppler broadened absorption profile.

The experimental setup is shown in Fig. 2. Short-pulse generation was achieved by focusing and spatially filtering light into an AOM operating at 400 MHz. As a result, the pulses have a temporal Gaussian profile with a FWHM of $\sim$20 ns. The resulting pulse bandwidth is much larger than the laser linewidth but smaller than the Doppler-broadened width of the transition.

Acoustic wave pulses are generated by rf pulses applied to the AOMs. We use phase-locked, voltage-controlled oscillators (VCO) to generate the rf frequencies used for driving the AOMs. The output of the VCO is turned on or off by transistor–transistor logic (TTL) switches and rf mixers connected in series. This arrangement ensures rf on/off ratios of $\sim$10,000:1. The corresponding on/off ratio for the optical pulses is measured to be $\sim$5000:1. The intensity of the background is mostly due to light that is 400 MHz off resonance and scattered into the excitation direction.

The TTL switches and the rf mixers are controlled by digital delay generators so that the delay time between the pulses can be varied with a precision of 1 ps. Another AOM operating at 260 MHz is placed before the 400 MHz AOM to upshift the laser frequency, as shown in Fig. 2. The 400 MHz AOM down shifts the laser frequency, shifting it on resonance. The rf period associated with the 400 MHz is 2.5 ns. Therefore, the time between the excitation pulses is varied in steps of exactly 2.5 ns to ensure that the rf pulse amplitude remains constant.

We use optical heterodyne detection to measure the amplitude of the electric field of the echo. This technique involves using a local oscillator (LO) beam that is derived by using a separate 260 MHz AOM, as shown in Fig. 2. The echo signal is combined with the LO on a beam splitter and directed into fast silicon *p-i-n* photodiodes (rise time of $<$1 ns). The photodiodes detect the echo by the presence of a 400 MHz beat note. This beat note is amplified, filtered, and sampled on a digital oscilloscope. Digital delay generators and VCOs are phase locked to a 10 MHz signal from a Rb atomic clock with a short-term stability of 5×10^{-11}. This arrangement allows heterodyne signal averaging by triggering the oscilloscope using TTL pulses from the delay generators. The heterodyne detection system was calibrated to ensure that the measured beat signal is a linear function of the echo signal amplitude and the detection system has a linear response for the range of our operating conditions.

The echo decay time can be measured by varying the time between the excitation pulses T and recording the

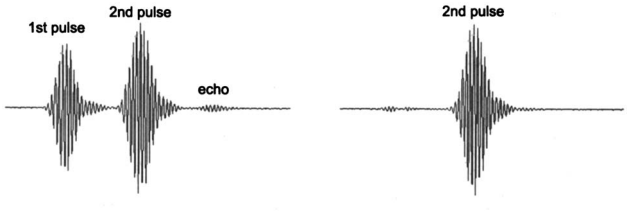

(a) Signal run (b) Background run (1st pulse off)

Fig. 3. Oscilloscope signal trace. (a) Signal run. (b) Background run (first pulse off).

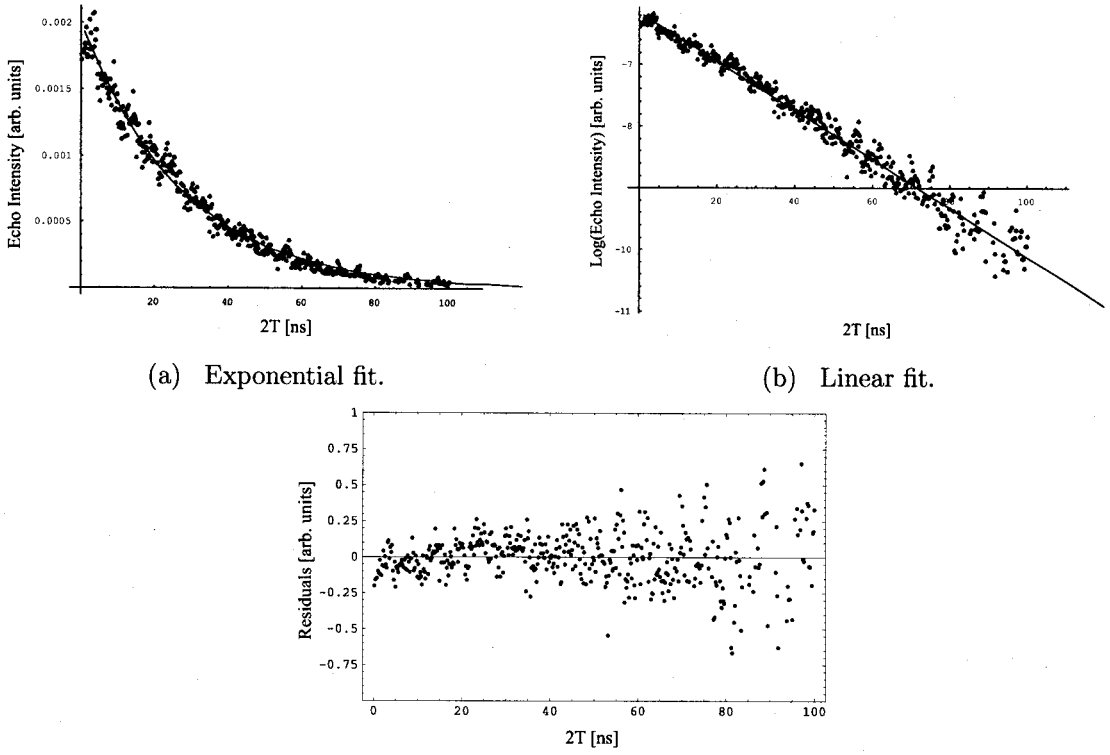

Fig. 4. Echo intensity fits. (a) Exponential decay of the echo intensity as a function of $2T$. (b) Natural logarithm of echo intensity as a function of $2T$ with linear fit. The slope results in a lifetime measurement of $\tau = 25.25 \pm 0.38$ ns. (c) Residuals: difference between data and fit for (b).

echo amplitude. For each data point, we average 128 repetitions of the experiment with both excitation pulses on and repeat the experiment with the first pulse turned off to obtain the background. In both cases, the oscilloscope traces shown in Fig. 3 are squared and integrated to obtain the echo intensity.

The result from the background trace is subtracted from the result of the signal trace. This quantity is proportional to the intensity of the echo and is plotted as a function of $2T$. Since the intensity is expected to show an exponential decay, as shown in Eq. (1), we fit the natural logarithm of the intensity as a function of $2T$ to a straight line. The negative inverse of the slope gives the excited-state lifetime [see Fig. 4(a) and 4(b)]. Residuals of the linear fit are shown in Fig. 4(c). We note that no systematic deviations from the fit were observed in all the data sets used in this work.

4. RESULTS AND DISCUSSION

We now discuss possible systematic effects that could affect the lifetime measurement. We varied the parameters affecting the echo intensity and measured the echo decay time constant. These include the intensity and durations of the excitation pulses, cell temperature, strength of a quantizing magnetic field, and the beam diameter of the excitation pulses.

Figures 5(a) and 5(c) show the effects on the echo lifetime by varying the width and the amplitude of the first pulse, respectively. These parameters define the pulse area of the first pulse. To vary the excitation-pulse amplitude and width, we adjust the voltage and duration of the control pulses connected to the TTL switches and mixers.

The horizontal axis represents the integrated intensity of the pulse recorded on a photodiode (pulse intensity). The data were fit to a straight line. The error in the slope is found to be larger than the absolute value of the slope. In this case it is reasonable to conclude that the slope is zero and that there is no systematic effect on the first pulse intensity.

We have used the same criterion to rule out systematic effects due to all the parameters listed above. The results pertaining to the cell temperature and the beam diameter are also shown in Fig. 5. The cell temperature was varied by adjusting the current through the tape heaters and by regulating the hot-air blower. Over the range of temperatures, the optical depth at line center was varied from ~ 0.7 to ~ 3. It is well known that increasing the vapor density can affect the propagation of the echo pulse,[21] but we do not expect or observe an effect on the decay time.

The quantizing magnetic field was varied between 0 to ~ 2 G by adjusting the current to the solenoid. Although the magnetic field affects the echo amplitude, it did affect the decay time.

The diameter of the excitation beams was varied between ~ 1 to ~ 2.5 mm and measured using a scanning-knife-edge beam profiler.[22] Assuming a Gaussian laser beam profile, it can be shown that the expression for the echo intensity including the effect of transit time decay is given by[23]

$$I' = \frac{(\pi a u)^4}{(7 + 10uT^2/a^2)^2} e^{-2T/\tau}. \quad (2)$$

Here, a is the $1/e^2$ beam radius and u is the most probable speed. The effective decay time extracted from Eq. (2) is plotted in Fig. 6 as a function of beam radius. The predictions of this model are consistent with the data in Fig. 5 and suggest that the effect of transit time decay is negligible for the beam sizes used.

Since we did not find any systematic trends, the final value for the lifetime was determined on the basis of a double-blind study by averaging 67 equally weighted data sets distributed between both ^{85}Rb and ^{87}Rb isotopes. The distribution of points is a Gaussian and is shown in Fig. 7 with an average value $\tau = 26.47 \pm 0.30$ ns. The quoted error represents the standard deviation of the mean (1σ uncertainty). The measurement has a precision of 1.14% and is in agreement at the level of 1σ with the best measurement in Rb[6] (26.20±0.09 ns). This measurement as well as our results disagree with a previous measurement of Ref. 24 at the 1σ level (27.0±0.5 ns).

A systematic effect that we have not tested for is the effect of collisional dephasing on the echo lifetime. Never-

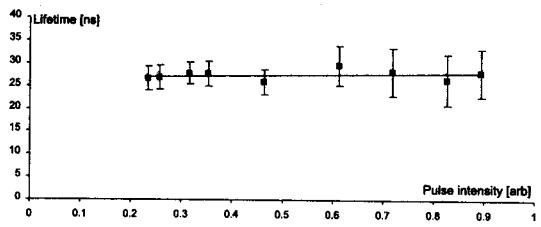

(a) 1st pulse width dependence.

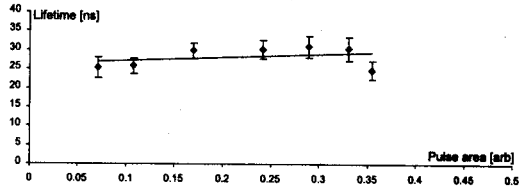

(b) 2nd pulse width dependence.

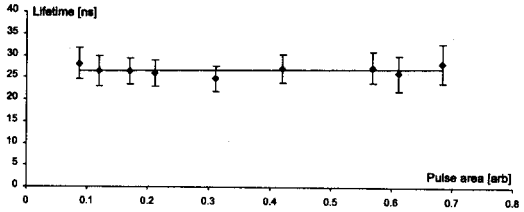

(c) 1st pulse amplitude dependence.

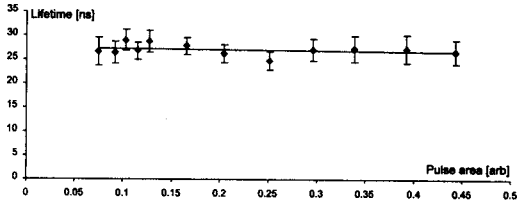

(d) 2nd pulse amplitude dependence.

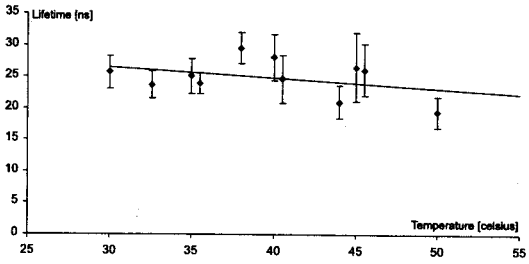

(e) Temperature dependence.

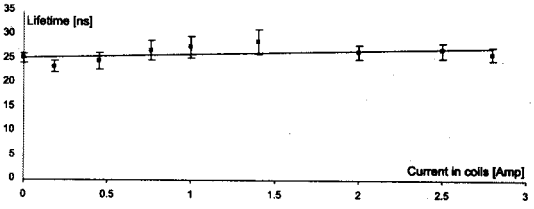

(f) Magnetic field current dependence.

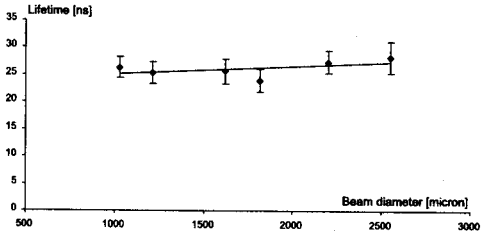

(g) Beam diameter dependence.

Fig. 5. Echo intensity dependence on (a) first pulse width, slope=1.142±3.862; (b) second pulse width, slope=8.539±26.999; (c) first pulse amplitude, slope=1.164±4.377; (d) second pulse amplitude, slope=−2.023±6.148; (e) temperature, slope=−0.162±0.334 ns/°C; (f) magnetic field current, slope=0.775±1.209 ns/A; (g) beam diameter, slope=0.00152±0.00305 ns/μm.

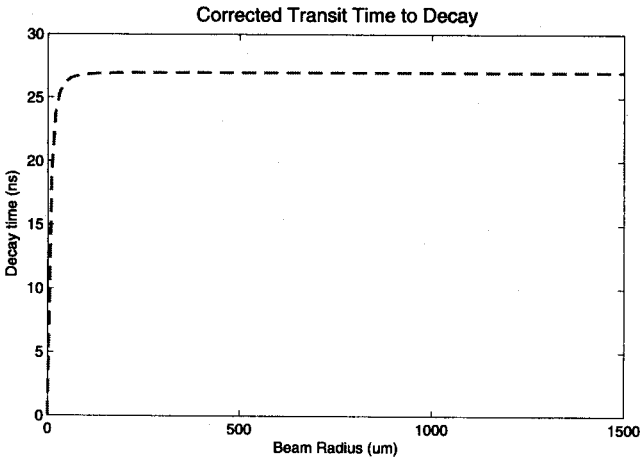

Fig. 6. Effective decay time due to transit time. Estimated correction to the decay time at the smallest beam size used is 0.03%, well below the sensitivity of the experiment. Range of beam radii used in the experiment is 500 to 1250 μm.

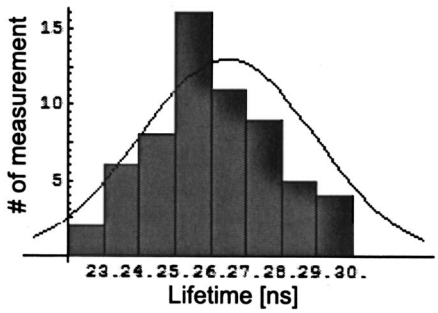

Fig. 7. Distribution of measurement points and Gaussian fit.

theless, it is possible to rule out this effect on the time scale of the experiment based on estimates. The base pressure of the vacuum system from which the Rb cell was made was $\sim 10^{-9}$ Torr. At the time the cell was sealed using an acetylene flame, the cell pressure was $\sim 1 \times 10^{-7}$ Torr. We note that the vapor pressure of Rb at room temperature is $\sim 3 \times 10^{-7}$ Torr. Absorption spectra confirm that under typical operating conditions, the pressure in the cell can be increased up to $\sim 10^{-6}$ Torr. For a typical alkali atom, it is well known that the collisional broadening rate for the principal resonance line is $\sim$10 MHz/Torr.[25] Therefore, it is clear that collisional effects can be ruled out on the time scale of the experiment ($\sim$100 ns). Similarly, based on the estimated amount of resonant background light, we rule out the effect of decoherence owing to background light along the direction of the excitation beams.

The experiment was carried out without optical pumping into a single magnetic sublevel. Optical pumping is expected to increase the signal-to-noise ratio but is not expected to affect the lifetime, because all the magnetic sublevels of the excited state have the same radiative decay rate.

5. STUDY OF ECHO INTENSITY

The behavior of the echo intensity as a function of the excitation pulse area is well understood in the absence of spontaneous emission.[18] Since our experiment involved pulse widths that are comparable to the lifetime and since the excitation beams have a finite spatial profile, we can expect that the dependence of the signal intensity will differ from the ideal case. Figure 8 shows the echo intensity versus the pulse area. This study is relevant to the lifetime measurement, as it allows the determination of experimental parameters that result in the highest signal-to-noise ratio. The quantity shown on the horizontal axis is obtained by integrating the square root of the excitation pulse intensities recorded by the photodiode and is therefore proportional to pulse area θ. The results show that the maximum echo intensity is obtained when the ratio $\theta_2/\theta_1 \sim 1.2$. In contrast, for the ideal case, the theory ignores the effect of spontaneous emission and the temporal and spatial profiles of the excitation beams so that this ratio is predicted to be 2.

The theory must be modified to include the effect of spontaneous emission and the Gaussian pulse shapes.[18] The effect of the spatial profile can also be taken into account by assigning a Gaussian distribution of Rabi frequencies and averaging the response over the profile. The details of the simulations are presented in Appendix A. The results of the simulations are shown in Fig. 9; they are qualitatively consistent with the data presented in Fig. 8.

6. CONCLUSIONS

In summary, we have carried out a measurement of the lifetime of the $5P_{3/2}$ level in Rb precise to 1.14% that agrees with the most precise measurement for this transition. Since each data set shown in Fig. 4 takes approximately 30 min, it is realistic to accumulate data sufficient for a 0.25% determination as in Refs. 5, 6, 8, and 9. This effort would require potential systematic effects to be reexamined at a higher level of precision. The work can also be immediately extended to the $5P_{1/2}$ transitions, so that comparisons with previous measurements are possible as in Ref. 9. The absence of systematic effects as well as the relative simplicity of this technique suggest that it is expected to be widely suitable for precision measurements in atomic and ionic transitions that have relatively large

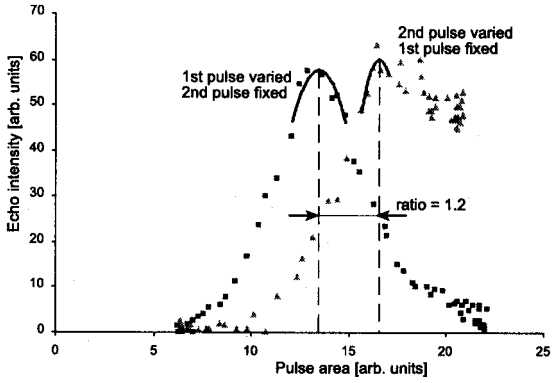

Fig. 8. Echo intensity measured as a function of first pulse area (squares), while keeping the second pulse area fixed at signal maximum; echo intensity measured as a function of second pulse area (triangles), while keeping the first pulse area fixed at signal maximum.

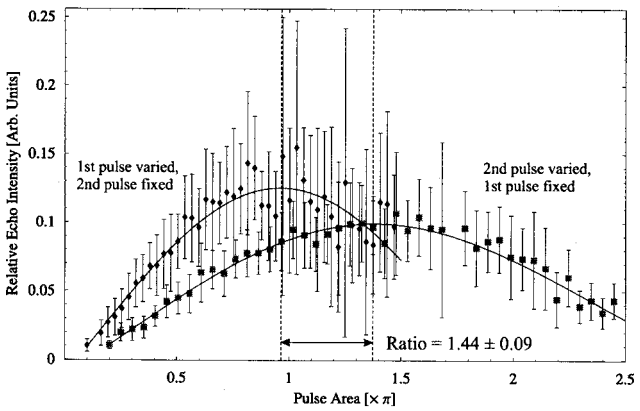

Fig. 9. Simulation of echo intensity as a function of pulse areas for temporally varying Gaussian pulses, including the effect of spontaneous emission and spatial intensity profile. These results correspond to case 3 in Appendix A. Ratio of the pulse areas that give maximum echo signals is $\theta_2/\theta_1=1.44\pm0.09$. Error in the measurement was computed from fit errors.

oscillator strengths. Since laser sources have become available in a wide spectral range, it is possible to implement this technique for accurate measurements of lifetimes in a variety of transitions.

APPENDIX A: MONTE CARLO SIMULATIONS OF THE PHOTON ECHO

The area theorem[18] for photon echoes does not appear to have been studied under realistic experimental conditions. The three examples discussed in this section allow a direct experimental test of the theorem.

To simulate the photon echo intensity, one can solve the optical Bloch equations for a large number of atoms, N, with each atom described by a set of Bloch vectors. The vector sum of the Bloch vectors is proportional to the echo amplitude. The square of the amplitude is proportional to the echo intensity,

$$I(\Delta t)\propto\left[\sum_{i=1}^{N}u_i(\Delta t)\right]^2+\left[\sum_{i=1}^{N}v_i(\Delta t)\right]^2+\left[\sum_{i=1}^{N}w_i(\Delta t)\right]^2, \tag{A1}$$

where Δt is the time with respect to the echo time ($t=t_1+t_2+2T$), T is the separation between the two pulses, and t_1 and t_2 are the widths of the first and second pulses, respectively. The population inversion w contains the difference between the excited-state and the ground-state populations. Components u and v are called the in-phase and in-quadrature components of the dipole matrix element $\langle d\rangle$, which can be expressed as[20]

$$\langle d\rangle=2\langle g|d|e\rangle[u\cos(\omega_L t)-v\sin(\omega_L t)].$$

Here $|g\rangle$ and $|e\rangle$ are the ground and excited states, respectively.

The optical Bloch equations under the rotating wave approximation (RWA) are given by the matrix equation[18]

$$\begin{bmatrix}\dot u(t)\\ \dot v(t)\\ \dot w(t)\end{bmatrix}=\begin{bmatrix}0 & -\Delta & 0\\ \Delta & 0 & \Omega_0(t)\\ 0 & -\Omega_0(t) & 0\end{bmatrix}\begin{bmatrix}u(t)\\ v(t)\\ w(t)\end{bmatrix}, \tag{A2}$$

where $\Delta\equiv\omega_L-\omega_0$ is the detuning of the laser from resonance and $\Omega_0(t)$ is the Rabi frequency. The Rabi frequency is related to the electric field envelope $\mathcal{E}(t)$ and the magnitude of the dipole matrix element by

$$\Omega_0(t)=\frac{2\langle d\rangle}{\hbar}\mathcal{E}(t).$$

If the Rabi frequency is constant in time, i.e., $\Omega_0(t)=\Omega_0$, then Eq. (A2) has an analytical solution[18]:

$$\begin{bmatrix}u(t)\\ v(t)\\ w(t)\end{bmatrix}=\begin{bmatrix}\dfrac{\Omega_0^2+\Delta^2\cos\Omega t}{\Omega^2} & -\dfrac{\Delta}{\Omega}\sin\Omega t & -\dfrac{\Delta\Omega_0}{\Omega^2}(1-\cos\Omega t)\\ \dfrac{\Delta}{\Omega}\sin\Omega t & \cos\Omega t & \dfrac{\Omega_0}{\Omega}\sin\Omega t\\ -\dfrac{\Delta\Omega_0}{\Omega^2}(1-\cos\Omega t) & -\dfrac{\Omega_0}{\Omega}\sin\Omega t & \dfrac{\Delta^2+\Omega_0^2\cos\Omega t}{\Omega^2}\end{bmatrix}\begin{bmatrix}u_0\\ v_0\\ w_0\end{bmatrix}. \tag{A3}$$

Here Ω is the generalized Rabi frequency given by

$$\Omega(\Delta)=\sqrt{\Omega_0^2+\Delta^2}.$$

The photon echo occurs as a result of rephasing of the velocity distribution excited by the first pulse. The velocity distribution produces a range of detunings within the sample. In the simulation this distribution is assumed to be Gaussian. The detuning is allowed to vary with velocity V_z along the direction of the laser beam,

$$\Delta(V_z)=\delta+\frac{V_z}{\lambda_L}.$$

The wavelength of the laser was set to the resonant wavelength of the atomic transition, and the detuning at zero velocity was set to $\delta=0.001\Gamma$, where $\Gamma=3.7\times10^7\ \mathrm{s}^{-1}$ is the radiative rate of the atomic transition. The velocity is chosen pseudorandomly for each atom in a Gaussian distribution centered at zero with a width defined by

$$V_0 = \sqrt{\frac{2k_B\mathcal{T}}{M_{\mathrm{Rb}}}}.$$

Here k_B is the Boltzmann constant, M_{Rb} is the atomic mass of Rb and the temperature of the atomic vapor, $\mathcal{T}$, was set to 20°C (273 K).

The laser beam is assumed to have a Gaussian intensity profile and is taken into account by letting the Rabi frequency vary with position as

$$\Omega_0(r) = \Omega_0 e^{-(r/r_0)^2}.$$

The e^{-2} radius of the laser beam, r_0, was set to 1 mm and the position r was chosen pseudorandomly in a Gaussian distribution centered at zero with a width of r_0.

We have simulated the echo intensity as a function of pulse area on three different cases: (1) with square pulses, (2) with Gaussian pulses, and (3) with Gaussian pulses and spontaneous emission. In all cases the simulation takes into account the spatial dependence of the Rabi frequency due to a Gaussian laser beam, and the Gaussian distribution of velocities. The simulations were performed by solving the optical Bloch equations for $N=10^4$ Bloch vectors. The pulse areas of both the $\pi/2$ and the π pulses were varied by changing the width of the pulses and keeping the amplitude fixed. Central values of $t_0=20$ ns were used so that the areas are $\pi/2$ and π for the first and second pulses, respectively. The pulse separation T was kept constant at 100 ns for all pulse widths in all three cases.

Case 1: Square Pulses

To simulate photon echoes with square pulses, the analytical solution to the optical Bloch equations under a steady field was used [Eq. (A3)]. The problem can be split into four time intervals: (1) $t\in[0,t_1]$, (2) $t\in[t_1,t_2]$, (3) $t\in[t_2,t_3]$, and (4) $t\in[t_3,t_{max}]$, where t_1, t_2, and t_3 are shown in Fig. 10, and t_{max} is sufficiently long to observe the echo, which occurs near $t=t_3+(t_2-t_1)$. Within intervals (1) and (3) the default Rabi frequency is set such that the pulse area was $\pi/2$ and π, respectively. In time intervals (2) and (4), the Rabi frequency is set to zero. The system is evolved from $t=0$ to t_{max} using the final conditions at the end of each interval as the initial conditions for the next interval.

The Rabi frequencies were set using the following relations:

$$\theta_1 = \Omega_1 t_0 = \frac{\pi}{2},$$

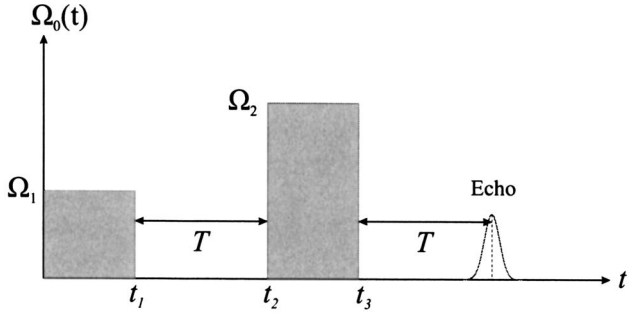

Fig. 10. Square pulse sequence.

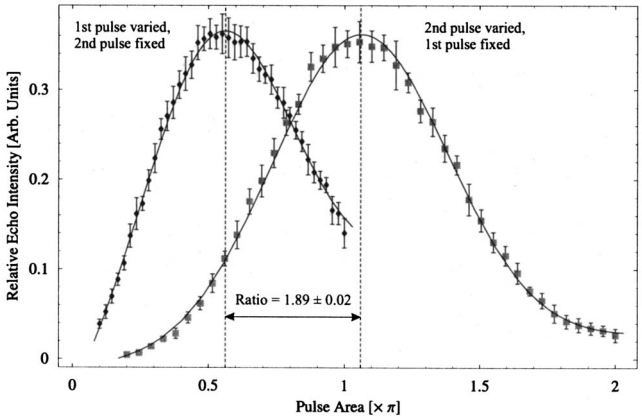

Fig. 11. Simulation of echo intensity as a function of pulse areas for case 1. Ratio of the pulse areas that give maximum echo signals is $\theta_2/\theta_1=1.89\pm0.02$. Error in the measurement was computed from fit errors.

$$\theta_2 = \Omega_2 t_0 = \pi,$$

where Ω_1 and Ω_2 are shown in Fig. 10. By setting $\Omega_1=\pi/(2t_0)$ and varying t_1 from $0.2t_0$ to $2.0t_0$, the first pulse area is varied from 0.1π to 1.0π. Similarly, by setting $\Omega_2=2\Omega_1$ and varying t_3-t_2 from $0.2t_0$ to $2.0t_0$, the second pulse area is varied from 0.2π to 2.0π. By plotting the echo intensity [Eq. (A1)] against pulse area we obtain Fig. 11. Each point on the graph has been averaged over ten separate runs, each of which corresponds to an average over 1000 Bloch vectors. The error bars were computed using the standard deviation of the ten runs averaged to obtain each point. The result is effectively the echo intensity for 10^4 Bloch vectors. The result is fit to the following function to obtain an accurate value of the pulse area that corresponds to the maximum echo intensity:

$$F(\theta) = A\exp\left[-\frac{(\theta-\theta_0)^2}{2\sigma^2}\right] + B\theta + C, \tag{A4}$$

where A, B, C, σ, and θ_0 are fit parameters. This function has a maximum occurring at $\theta=\theta_{max}$, which is the solution to the equation

$$(\theta-\theta_0)\exp\left[-\frac{(\theta-\theta_0)^2}{2\sigma^2}\right] = \frac{\sigma^2 B}{A}.$$

The solution can be approximated as

$$\theta_{max} = \theta_0 + \frac{\sigma^2 B}{A}, \tag{A5}$$

which contains only fit parameters. Equation (A5) is used to estimate the area for which the echo signal is a maximum. An associated error for θ_{max} is computed using the error estimates from the fit parameter results:

$$(\delta\theta_{max})^2 = (\delta\theta_0)^2 + \left(\frac{2\sigma B}{A}\delta\sigma\right)^2 + \left(\frac{\sigma^2}{A}\delta B\right)^2 + \left(\frac{\sigma^2 B}{A^2}\delta A\right)^2.$$

Thus, from the fits we find the peak areas to be $\theta_1=(0.561\pm0.005)\pi$ and $\theta_2=(1.063\pm0.003)\pi$. The ratio of the peaks is then computed to be $\theta_2/\theta_1=1.894\pm0.019$, which is significantly less than the analytical result[18] of

$\theta_2/\theta_1=2$. This result can be attributed primarily to the effect of the spatial profile of the excitation beam.

Case 2: Gaussian Pulses

To simulate photon echoes with Gaussian pulses we could no longer use the analytical result of Eq. (A3), since the Rabi frequency is not steady in time. Instead we numerically solved the optical Bloch equation (A2) with a Rabi frequency given by

$$\Omega_0(r,t)=\left\{\Omega_1\exp\left[-\frac{(t-t_{01})^2}{2\sigma_1^2}\right]+\Omega_2\exp\left[-\frac{(t-t_{02})^2}{2\sigma_2^2}\right]\right\}\times\exp\left[-\left(\frac{r}{r_0}\right)^2\right]. \quad \text{(A6)}$$

Here, σ_1 and σ_2 are the standard deviations of the Gaussians. Ω_1, Ω_2, t_{01}, and t_{02} are as shown in Fig. 12. The FWHM of the pulses (t_1 and t_2) can be expressed in terms of σ_1 and σ_2:

$$t_1=2\sqrt{2\ln(2)}\sigma_1,$$

$$t_2=2\sqrt{2\ln(2)}\sigma_2.$$

By normalizing the Gaussians in Eq. (A6) with FWHM of $t_0=20$ ns, the Rabi frequency amplitudes Ω_1 and Ω_2 are found to be

$$\Omega_1=\sqrt{\frac{\pi}{2}}\frac{1}{2\sigma_0},$$

$$\Omega_2=2\Omega_1,$$

$$\sigma_0=\frac{t_0}{2\sqrt{2\ln(2)}}.$$

Then the pulse areas are

$$\theta_1=\sqrt{2\pi}\Omega_1\sigma_1=\frac{\sigma_1}{2\sigma_0}\pi=\frac{t_1}{2t_0}\pi,$$

$$\theta_2=\sqrt{2\pi}\Omega_2\sigma_2=\frac{\sigma_2}{\sigma_0}\pi=\frac{t_1}{t_0}\pi.$$

The FWHM of the pulses were varied from $t_1,t_2\in[0.2t_0,2.0t_0]$ with a constant step size, which is equivalent to varying the pulse areas from $\theta_1\in[0.1\pi,1.0\pi]$ and $\theta_2\in[0.2\pi,2.0\pi]$.

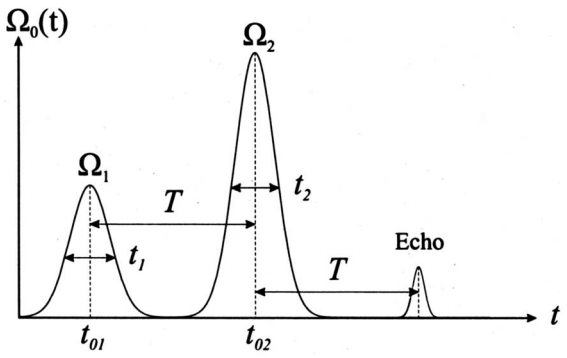

Fig. 12. Gaussian pulse sequence.

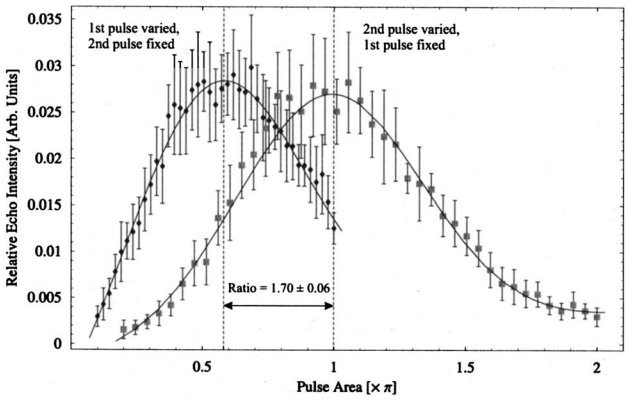

Fig. 13. Simulation of echo intensity as a function of pulse areas for case 2. Ratio of the pulse areas that give maximum echo signals is $\theta_2/\theta_1=1.70\pm0.06$. Error in the measurement was computed from fit errors.

The results were fit to the same function [Eq. (A4)] from which the peak areas were extracted as $\theta_1=(0.584\pm0.021)\pi$ and $\theta_2=(0.993\pm0.009)\pi$, with a ratio of $\theta_2/\theta_1=1.701\pm0.063$ (Fig. 13). The ratio has further decreased from 1.89 to 1.70, which can be attributed solely to the effect of Gaussian pulses used in this simulation.

Case 3: Gaussian Pulses with Spontaneous Emission

To incorporate spontaneous emission into the simulation the optical Bloch equation (A2) must be modified to include phenomenological decay constants[18]:

$$\dot{u}(t)=-\frac{u(t)}{\tau_2}-\Delta v(t),$$

$$\dot{v}(t)=\Delta u(t)-\frac{v(t)}{\tau_2}+\Omega_0 w(t),$$

$$\dot{w}(t)=-\Omega_0 v(t)-\frac{w(t)}{\tau_1}+\frac{w_{eq}}{\tau_1}. \quad \text{(A7)}$$

Here, $\tau_1=\Gamma^{-1}$ is the population decay time, $\tau_2=2\tau_1$ is the coherence decay time, and $w_{eq}=-1$ is the value to which the population inversion relaxes after long times due to spontaneous emission.

The numerical solution to Eq. (A7) is averaged over a large number of atoms; the simulation is otherwise performed in the same manner as in case 2. The results of this simulation are shown in Fig. 9. From the fits we find $\theta_1=(0.962\pm0.018)\pi$ and $\theta_2=(1.384\pm0.086)\pi$, with a ratio of $\theta_2/\theta_1=1.438\pm0.093$. The ratio decreases further in comparison with cases 1 and 2 solely due to spontaneous emission. However, it is only qualitatively in agreement with the data presented in Fig. 8.

ACKNOWLEDGMENTS

This work was supported by Canada Foundation for Innovation, Ontario Innovation Trust, Natural Sciences and

Engineering Research Council of Canada, Photonics Research Ontario, and York University.

A. Kumarakrishnan's e-mail address is akumar@yorku.ca.

REFERENCES

1. D. L. Moehring, B. B. Blinov, D. W. Gidley, R. N. Kohn, M. J. Madsen, T. B. Sanderson, R. S. Vallery, and C. Monroe, "Precision lifetime measurement of a single trapped ion with ultrafast laser pulses," Phys. Rev. A **73**, 023413 (2006).
2. M. S. Safronova, C. J. Williams, and C. W. Clark, "Relativistic many-body calculations of electric-dipole matrix elements, lifetimes and polarizabilities in rubidium," Phys. Rev. A **69**, 022509 (2004).
3. S. A. Blundell, W. R. Johnson, and J. Sapirstein, "Relativistic all-order calculations of energies and matrix elements in cesium," Phys. Rev. A **43**, 3407–3418 (1991).
4. V. A. Dzuba, V. V. Flambaum, A. Y. Krafmakher, and O. P. Sushkov, "Summation of the high orders of perturbation theory in the correlation correction to the hyperfine structure and to the amplitudes of $E1$-transitions in the cesium atom," Phys. Lett. A **142**, 373–377 (1989).
5. C. W. Oates, K. R. Vogel, and J. L. Hall, "High precision linewidth measurement of laser-cooled atoms: resolution of the Na $3p\ ^2P_{3/2}$ lifetime discrepancy," Phys. Rev. Lett. **76**, 2866–2869 (1996).
6. J. E. Simsarian, L. A. Orozco, G. D. Sprouse, and W. Z. Zhao, "Lifetime measurements of the $7p$ levels of atomic francium," Phys. Rev. A **57**, 2448–2458 (1998).
7. W. I. McAlexander, E. R. I. Abraham, and R. G. Hulet, "Radiative lifetime of the $2P$ state of lithium," Phys. Rev. A **54**, R5–R8 (1996).
8. U. Volz and H. Schmoranzer, "Precision lifetime measurements on alkali atoms and on helium by beam-gas-laser spectroscopy," Phys. Scr., T **T65**, 48–56 (1996).
9. L. Young, W. T. Hill III, S. J. Sibener, S. D. Price, C. E. Tanner, C. E. Wieman, and S. R. Leone, "Precision lifetime measurements of Cs $6p\ ^2P_{1/2}$ and $6p\ ^2P_{3/2}$ levels by single-photon counting," Phys. Rev. A **50**, 2174–2181 (1994).
10. C. K. N. Patel and R. E. Slusher, "Photon echoes in gases," Phys. Rev. Lett. **20**, 1087–1089 (1968).
11. A. Flusber, T. Mossberg, and S. R. Hartman, "Excited-state photon-echo relaxation in Na vapor," Opt. Commun. **24**, 207–210 (1978).
12. R. A. Forber, L. Spinelli, J. E. Thomas, and M. S. Feld, "Observation of quantum diffractive velocity-changing collisions by use of two-level heavy optical radiators," Phys. Rev. Lett. **50**, 331–335 (1990).
13. Y. C. Chen, K. Chiang, and S. R. Hartmann, "Spectroscopic and relaxation character of the $^3P_0$-$^3H_4$ transition in LaF_3:Pr^{3+} measured by photon echoes," Phys. Rev. B **21**, 40–47 (1980).
14. R. M. Macfarlane and R. M. Shelby, "Sub-kilohertz optical linewidths of the $^7F_0 \Leftrightarrow {}^5D_0$ transition in Y_2O_3:Eu^{3+}," Opt. Commun. **39**, 169–171 (1981).
15. P. C. Becker, H. L. Fragnito, C. H. Brito Cruz, R. L. Fork, J. E. Cunningham, J. E. Henry, and C. V. Shank, "Femtosecond photon echoes from band-to-band transitions in GaAs," Phys. Rev. Lett. **61**, 1647–1649 (1988).
16. E. L. Hahn, "Spin echoes," Phys. Rev. **80**, 580–594 (1950).
17. I. D. Abella, N. A. Kurnit, and S. R. Hartmann, "Photon echoes," Phys. Rev. **141**, 391–406 (1965).
18. L. Allen and J. H. Eberly, *Optical Resonance and Two-Level Atoms* (Wiley, 1975).
19. C. Cohen-Tannoudji, J. Dupont-Roc, and G. Grynberg, *Photons and Atoms* (Wiley-Interscience, 1997).
20. C. Cohen-Tannoudji, J. Dupont-Roc, and G. Grynberg, *Atom-Photon Interactions* (Wiley-Interscience, 1998).
21. S. L. McCall and E. L. Hahn, "Self-induced transparency," Phys. Rev. **183**, 457–485 (1969).
22. A. E. Siegman, *Lasers* (University Science Books, 1986).
23. A. Kumarakrishnan, U. Shim, S. B. Cahn, and T. Sleator, "Ground-state grating echoes from Rb vapor at room temperature," Phys. Rev. A **58**, 3868–3872 (1998).
24. A. Gallagher and E. L. Lewis, "Resonance broadening of Hanle-effect signals in rubidium," Phys. Rev. A **10**, 231–241 (1974).
25. N. Allard and J. Kielkopf, "The effect of neutral nonresonant collisions on atomic spectral lines," Rev. Mod. Phys. **54**, 1103–1182 (1982).